Applied Catalysis B: Environmental 222 (2018) 182–190

Contents lists available at ScienceDirect

Applied Catalysis B: Environmental

journal homepage: www.elsevier.com/locate/apcatb

Catalysts synthesized by selective deposition of Fe onto Pt for the water-gas shift reaction

Isaias Barbosa Aragao[a,b], Insoo Ro[b], Yifei Liu[b], Madelyn Ball[b], George W. Huber[b], Daniela Zanchet[a,*], James A. Dumesic[b,*]

[a] Institute of Chemistry, University of Campinas (UNICAMP), P.O. Box 6154, 13083-970 Campinas, São Paulo, Brazil
[b] Department of Chemical and Biological Engineering, University of Wisconsin-Madison, 1415 Engineering Drive, Madison, WI 53706, United States

ARTICLE INFO

Keywords:
Bimetallic catalyst
FePt
Controlled surface reactions (CSR)
Water-gas shift reaction (WGSR)

ABSTRACT

FePt bimetallic catalysts with intimate contact between the two metals were synthesized by controlled surface reactions (CSR) of (cyclohexadiene)iron tricarbonyl with hydrogen-treated supported Pt nanoparticles. Adsorption of the iron precursor on a Pt/SiO_2 catalyst was studied, showing that the Fe loading could be increased by performing multiple CSR cycles, and the efficiency of this process was linked to the renewal of adsorption sites by a reducing pretreatment. The catalytic activity of these bimetallic catalysts for the water gas shift reaction was improved due to promotion by iron, likely linked to H_2O activation on FeO_x species at or near the Pt surface, mostly in the (II) oxidation state.

1. Introduction

The catalytic properties of bimetallic systems can present chemical and physical behaviors that are more than just a sum of their separate parts [1], leading to orders of magnitude enhancement in activities and selectivities compared to their monometallic counterparts [2–4]. However, the creation of a narrow distribution of surface sites represents a challenge for typical deposition methods, which often create a wide composition range, making it difficult to rationalize the system and elucidate the nature of the active sites.

The synthesis of bimetallic catalyst systems has been explored in the literature using colloidal methods [5] and heterometallic clusters [6–11]. Some of the limitations of these approaches include the presence of strongly bonded capping molecules, e.g., organic acids or amines, to the surface of the nanoparticles (NPs), or atmosphere-sensitive reactions for the synthesis of precursors. A method employing controlled surface reactions (CSR) represents an alternative to overcome some of these issues by selectively depositing a commercial organometallic complex on the surface of preformed NPs [12–16]. The CSR method has been successfully applied to synthesize bimetallic systems, revealing promotion effects that can be several orders of magnitude higher than the monometallic unpromoted catalysts. In the case of carbon-supported MoPt catalysts made by the CSR approach, for example, there was a 4000 fold increase in activity for the water gas shift reaction (WGSR), raising the potentiality of the method [12].

One bimetallic system of particular interest in which the CSR method could be successfully explored is FePt, which has shown excellent performance in several key reactions [17–19]. For example, Zhang et al. [17] studied the oxidation of CO in H_2-rich gas mixtures (PROX-CO) and showed that Fe-decorated Pt NPs became more active at low temperatures due to the change in reaction mechanism. While Pt NPs follow a competitive Langmuir-Hinshelwood mechanism, the presence of Fe moieties leads to a non-competitive bi-functional mechanism, by preferentially activating the O_2. This change in mechanism due to the oxophyllic properties of the FeO_x moieties is ubiquitous [20–22] and has also been shown on other Fe bimetallic systems [23,24].

For the WGSR, in which H_2O activation is a rate limiting step for several systems, different bimetallic systems have already been studied [25–31] aiming to improve selectivity and conversion. In this paper, we explore the CSR method to synthesize FePt catalysts for the WGSR. In particular, a detailed study on the parameters that affect the Fe deposition was performed, shedding light on the requisites to selectively deposit the iron moieties on Pt NPs.

2. Experimental

SiO_2 (Davisil grade 646, Sigma-Aldrich) was used as support for the catalysts. It was crushed and sieved to 60–100 mesh (0.150 − 0.250 mm), then stirred with 20% HNO_3 for 3 h, vacuum filtered, washed until pH 7 with milli-Q grade H_2O, and dried overnight at 383 K before use. Alumina (γ-Al_2O_3, CATALOX SBA-200) and titania

* Corresponding authors.
E-mail addresses: daniela@iqm.unicamp.br (D. Zanchet), jdumesic@wisc.edu (J.A. Dumesic).

http://dx.doi.org/10.1016/j.apcatb.2017.10.004
Received 14 July 2017; Received in revised form 9 September 2017; Accepted 3 October 2017
Available online 04 October 2017
0926-3373/

(TiO_2, P25, Degussa) were used as received. (Cyclohexadiene)iron tricarbonyl ($C_6H_8Fe(CO)_3$, Strem Chemicals, 98%), and anhydrous *n*-pentane (Sigma-Aldrich) were used without further purification, handled and stored under inert gas inside a glovebox. Chloroplatinic acid hexahydrate ($H_2PtCl_6{\cdot}6H_2O$, Sigma-Aldrich, ≥37.50% Pt basis) and iron(III) nitrate nonahydrate ($Fe(NO_3)_3{\cdot}9H_2O$, Strem, 98 +%) were used as precursors for incipient wetness impregnation (IWI).

2.1. Synthesis

A monometallic catalyst containing 5 wt% Pt, which will be referred as 5Pt/SiO_2, was synthesized by IWI, as described elsewhere [12]. Briefly, 1.2 mL of a solution containing the desired amount of Pt precursor to achieve 5 wt% was added to each gram of SiO_2. The solid was dried at 383 K for 3 h, and the final solid was reduced at 533 K (1 K min^{-1}) for 4 h under 100 mL min^{-1} of H_2 (Industrial grade, Airgas) and passivated at room temperature under 100 mL min^{-1} of 1% O_2/He. A Pt/C monometallic catalyst was synthesized following the same procedure.

The CSR method was used to prepare bimetallic catalysts [13]. In a typical synthesis, using Schlenck line techniques and a glove box, 0.7 g of 5Pt/SiO_2 catalyst was reduced at 573 K for 4 h (1 K min^{-1}) under 100 mL min^{-1} of H_2. Then, 3.5 g of pentane solution containing 0.714 mg gcat^{-1} of (cyclohexadiene)iron tricarbonyl (equivalent to 0.05:1 Fe:Pt, 0.07 wt% of Fe) was added and left stirring for 2 h. The excess solvent was removed, the residue was vacuum dried, and the remaining solid was reduced again at 573 K. At this stage, the sample was passivated at room temperature under 100 mL min^{-1} of 1% O_2/He to produce the final catalyst or reduced again and transferred to the glove box to perform a new CSR cycle targeting higher Fe loadings. A hydrogen pretreatment step was performed between cycles, unless noted otherwise. After the final passivation step, the sample was handled under ambient conditions.

A batch of catalyst was prepared without any hydrogen pretreatment to evaluate the influence of this procedure on adsorption of the precursor. In this case, the pre-reduced Pt/SiO_2 catalyst was degassed overnight under vacuum at room temperature, followed by refilling with Ar and precursor deposition.

Catalysts made by CSR on Pt/SiO_2 were denoted as Pt_1Fe_A/SiO_2_BC, in which A corresponds to the final 1 Pt: A Fe molar ratio (nominal values from 0.05 to 0.2) and B is the number of cycles (1–6) performed to achieve that Fe loading; for example, $Pt_1Fe_{0.2}/SiO_2$_4C was prepared by 4 cycles using 0.05 equivalents of Fe, with a final ratio of 0.2. In the case of $Pt_1Fe_{0.2}/SiO_2$_1C, the solvent was evaporated so the desired Fe:Pt ratio could be achieved using one cycle. The catalyst composition was determined by ion coupled plasma-atomic emission spectroscopy (ICP-AES). The CSR method was applied to the Pt/C catalyst to produce the $Pt_1Fe_{0.2}$/C_1C catalyst. The same CSR procedure was applied to the SiO_2 support to produce Fe/SiO_2, in which the amount of Fe was equivalent to $Pt_1Fe_{0.2}/SiO_2$_1C. Control experiments were carried out in which the CSR method was used for SiO_2, TiO_2, and γ-Al_2O_3. For comparison, a bimetallic FePt catalyst was prepared by IWI (IWI-$Pt_1Fe_{0.2}/SiO_2$), where the desired amount of iron nitrate was added to Pt/SiO_2, and the solid was dried overnight and calcined for 4 h at 563 K under air (1 K min^{-1}).

2.2. Characterization

2.2.1. Electronic spectroscopy

Electronic spectra (UV–vis) were acquired in a Thermo Scientific Evolution 300 UV–vis spectrometer. Samples were prepared in *n*-pentane in a glove box. Precursor adsorption (% adsorbed and amount of Fe adsorbed) was measured by the concentration of precursor in solution after the CSR procedure using a calibration curve of the absorbance maximum at 290 nm, Fig. S1.

2.2.2. CO-Chemisorption

The CO chemisorption studies were performed using a Micromeritics ASAP2020C apparatus. Prior to measurement of the CO uptake at 303 K, the catalyst was reduced in flowing H_2 at 573 K for 2 h. Metallic surface area was calculated assuming the adsorption of 1 CO molecule per Pt atom at the surface, as previously reported [16].

2.2.3. X-Ray diffraction

Powder X-Ray Diffraction (XRD) patterns were acquired on a Bruker D8 Discovery, operating with Cu-Kα micro X-ray source, with a Montel mirror, and a Vantec 500 area detector.

2.2.4. Atomic emission spectroscopy

ICP-AES was performed with a Perkin-Elmer Plasma 400 ICP Emission Spectrometer. Fifty mg of each sample was digested with 10 g of aqua regia overnight at 423 K in a reflux system, and then diluted with milli-Q grade water and quantified. Calibration curves were made with commercial ICP standards − Pt and Fe in hydrochloric acid from TraceCERT®, Sigma-Aldrich.

2.2.5. Electron microscopy

Samples were deposited on holey carbon Cu TEM grids by dropping an ethanol suspension of each sample on it, followed by plasma cleaning before analysis. A FEI Titan STEM with Cs probe aberration corrector operated at 200 kV with spatial resolution < 0.1 nm was used for scanning transmission electron microscopy (STEM) studies. High-angle annular dark-field (HAADF) images were collected with detector angle ranging from 54 to 270 mrad, probe convergence angle of 24.5 mrad, and probe current of approximately 25 pA. Energy dispersive x-ray spectroscopy (EDS) data were collected using the same microscope with an EDAX SiLi Detector. EDS point spectra were collected with a probe current ~200-780 pA and spatial resolution ~0.5 nm. For each sample, approximately 50 NPs were analyzed by placing the beam on individual particles and collecting EDS spectra.

2.2.6. X-ray absorption fine structure

Ex situ X-ray Absorption Fine Structure (XAFS) measurements for the Fe K-edge were carried out at the 12BM at the Advanced Photon Source (APS) at the Argonne National Laboratory. The samples were reduced in an inert cell, sealed between Kapton® tapes inside of a glovebox, and kept in a sealed vial under inert atmosphere until the measurements. The samples were mounted in a slide support and the spectra were collected in fluorescence mode using a Canberra 13-Element Ge Detector.

In situ XAFS measurements at the Pt L_3-edge and Fe K-edge were acquired at XAFS2 beamline at the Brazilian Synchrotron Light Laboratory (LNLS), using a homemade tubular furnace operating in transmission mode. EXAFS (Extended X-ray Absorption Fine Structure) spectra were collected before and after reduction (573 K, 2 K min^{-1} under 100 mL min^{-1} at 5% H_2/He) at the Pt L_3-edge at room temperature. The temperature programmed reduction profile of one of the samples was done by X-ray Absorption Near Edge Structure (TPR-XANES) at the Fe K-edge (100 mL min^{-1} of 5% H_2/He, heating ramp to 873 K at 10 K min^{-1} scan time = 9 min). Spectra were collected under *in situ* WGSR conditions at both edges starting from the reduced catalysts, with CO:H_2O equal to 1:3 (6.6 mL min^{-1} of 5% CO in He, 0.99 mL min^{-1} of H_2O, and He as balance), with total flow of 100 mL min^{-1}.

XAFS data were analyzed using DEMETER 0.9.25 package software following standard procedure [32]. To evaluate the variation of the iron oxidation state, we applied the method proposed by Capehart et al. [33], in which the average oxidation state is correlated to the absorption edge shift obtained by the integration of the vacant electronic sites above the Fermi level in comparison with the standards.

2.3. Reaction kinetics measurements

The apparatus for studies of the WGSR was described elsewhere [12]. Briefly, 0.1–2.1 g of catalyst, diluted to 2.1 g with crushed SiO_2-chips, was reduced under 75 mL min^{-1} of 35% H_2/He at 573 K (2 K min^{-1}) for 2 h and then cooled to the reaction temperature (543 or 623 K). The reaction mixture consisted of 10 mol% CO, purified by passing through a column filled with silica chips held at 523 K, and 20 mol% H_2O, fed with a syringe pump (Harvard Apparatus PHD Ultra), with a total flow rate of 100 mL min^{-1} balanced with He. The conversion was measured online with a Shimadzu GC-8A equipped with a thermal conductivity detector (TCD) and Alltech HayeSep DB column to quantify CO and CO_2. Turnover frequencies (TOF) were determined for all reactions at conversions below 10% by normalizing the rate to the number of Pt sites determined by CO-chemisorption. If deactivation was observed, the TOF value reported was the TOF at zero time, obtained by plotting the ln(TOF) versus time and linearly extrapolating the TOF at zero time.

3. Results

3.1. Synthesis

In the CSR method, the organometallic precursor can react (i) selectively, with Pt NPs surface, which is the goal of the method, and/or (ii) unselectively, with hydroxyls from the support surface or with pore trapped environmental contaminants (such as O_2 and H_2O from the atmosphere or H_2 from the pretreatment). In addition, part of the precursor could adsorb on the surface of the support or remain in the reaction media, without reacting. These possibilities can be assessed by quantification of the precursor concentration by UV–vis, before and after the CSR approach. The success of the process is achieved by the selective deposition of the precursor onto the surface available sites of the Pt-NPs.

The parent Pt/SiO_2 catalyst used in this work was composed of Pt-NPs with average size of 5.4 nm, determined from STEM. CO-chemisorption resulted in 49.9 μmol g^{-1} of available sites, equivalent to 20% dispersion. The analysis of the UV–vis spectra taken before and after CSR using (cyclohexadiene)iron tricarbonyl (0.07 wt% of Fe) and Pt/SiO_2 confirmed successful deposition, Fig. 1. The remaining concentration of the precursor in the final solution was calculated through a calibration curve, Fig. S1, showing that more than 95% of the iron precursor deposited onto Pt in the Pt/SiO_2 catalyst (Fig. 1a), producing the catalyst $Pt_1Fe_{0.06}/SiO_2$_1C, as confirmed by ICP-AES. No indication

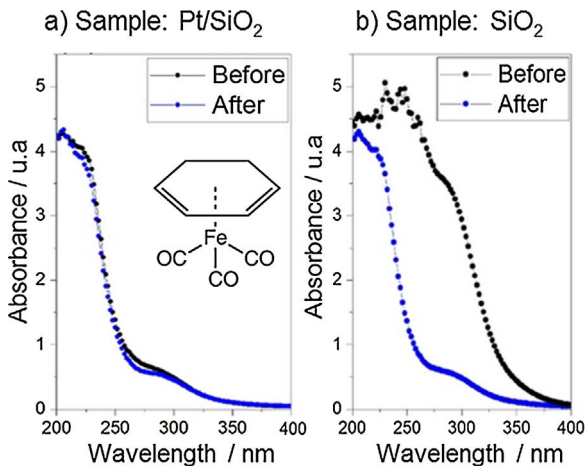

Fig. 1. UV–vis absorption spectra of Fe precursor solution before/after deposition onto a) Pt/SiO_2 and b) SiO_2. Note that while in a) there is a significant change in the absorbance, in b) no variation was detected. In b), the solutions were diluted prior the UV–vis measurements to be in the linear range of the calibration curve.

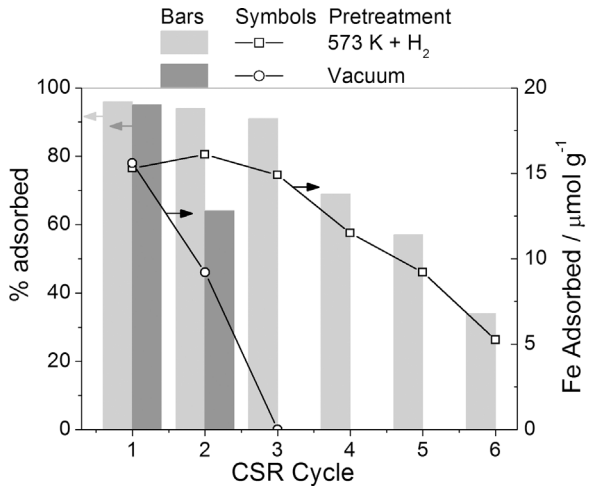

Fig. 2. Amount of precursor adsorbed at each CSR cycle (standard pretreatment under H_2 at 573 K). The results obtained with vacuum pretreatment are shown for comparison.

of reaction was detected when the iron precursor was exposed to the bare support (Fig. 1b). The iron precursors did deposit onto Al_2O_3 and TiO_2 as shown in Fig. S2.

Efforts to increase the Fe loading in a single cycle by using a higher precursor concentration (> 1 × 0.1) resulted in incomplete deposition, as detected by the presence of remaining precursor in solution and by comparing the Fe/Pt ratio detected by EDS and ICP-AES [34,35]. Multiple cycles of the organometallic precursor were performed to overcome this limitation. The amount of Fe deposited and the effectiveness of the deposition (% adsorbed) at each cycle were assessed, as can be seen in Fig. 2 and Table S1. For the first cycle, 95 +% adsorption of the precursor which corresponds to deposition of about 15 μmol of precursor per g of catalyst (where values were calculated in comparison to the nominal value of the initial concentration, 0.714 mg g^{-1}). This amount of Fe corresponds to about 30% of the available Pt surface sites for the Pt/SiO_2 catalyst. In addition, this value is in agreement with the reduction in the metallic area observed by CO chemisorption after the 1st CSR cycle (Fig. 3), indicating the occurrence of selective anchoring of the precursor on the Pt surface. We note that the hydrogen

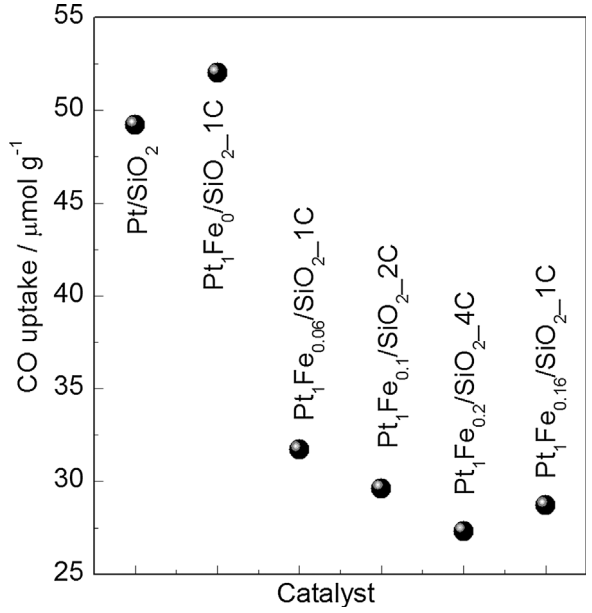

Fig. 3. CO-Chemisorption of the catalysts made by CSR in comparison to the monometallic Pt/SiO_2 and a blank CSR catalyst (Pt_1Fe_0/SiO_2_1C), produced after one CSR cycle without the addition of iron precursor.

pretreatments before and after CSR did not cause sintering of the Pt-NPs, Fig. S3, and therefore, could not explain the decrease in CO-chemisorption uptake.

In the third cycle, 95 +% of the precursor was adsorbed as shown in Fig. 2. In subsequent cycles, 4, 5 and 6, the deposition efficiency was reduced to approximately 70%, 60% and 35%, respectively. Saturation of the Pt sites with Fe should be achieved between the 3rd and 4th cycles when comparing the number of Pt sites available with the total amount of Fe deposited (Table S1). The total amount of Fe anchored after the 6th CSR cycle was 72.3 μmol g^{-1}, which corresponds to about 150% of the total metallic area. A control experiment was performed by pretreating the passivated Pt/SiO_2 catalyst under vacuum at room temperature to understand the mechanism of Fe deposition. The same amount of Fe deposition occurred on the first cycle, but the amount of Fe deposition dropped to half in the 2nd cycle. No measurable Fe deposition ocurred in the 3rd cycle. The total amount of Fe deposited during all three cycles corresponds to about half of the Pt sites. These observations suggest that the reductive treatment helps to renew the Pt sites available for the Fe deposition.

Despite the increase in Fe loading achieved by multiple CSR cycles, CO chemisorption showed a much smaller effect, with minor changes in the Pt metallic area after the 1st cycle (Fig. 3). Moreover, the sample $Pt_1Fe_{0.16}/SiO_2$_1C prepared by a single cycle showed CO-chemisorption of 28.7 μmol g^{-1}, close to the limit achieved by $Pt_1Fe_{0.1}/SiO_2$_2C and $Pt_1Fe_{0.2}/SiO_2$_4C, 29.6 and 27.3 μmol g^{-1}, respectively. For comparison, a catalyst was prepared by wet impregnation, IWI-$Pt_1Fe_{0.2}/SiO_2$ catalyst, and showed similar CO chemisorption value (Table S3).

Quantitative analysis of the amount of Fe and Pt carried out by EDS-STEM measurements of individual NPs particles, Fig. 4 and Fig. S4, showed good agreement between the average amount of Fe and the value measured by ICP-AES. The Fe/Pt ratio was dependent on the particle size, Fig. 4, where small particles have a higher Fe/Pt ratio than larger particles. This is expected in view of the geometric dependency between volume and surface area. To better visualize this dependency, a geometrical model was built in which the surface of a half-spherical Pt-NP was covered with a monolayer of Fe atoms and the total Fe atom % was calculated (see Supporting information for details).

TPR-XANES measurements were performed at the Fe K-edge to probe the nature of Fe sites generated in CSR, and results are presented in Fig. 5. At room temperature the XANES profile of the passivated $Pt_1Fe_{0.2}/SiO_2$_4C catalyst resembles the γ-Fe_2O_3 standard (Fig. 5a) with edge value of 7126.5 eV (in comparison to 7127.2 eV for the standard) and similar shape of the pre-edge peak. However, differences are visible, and although it is not possible to determine the oxidation state

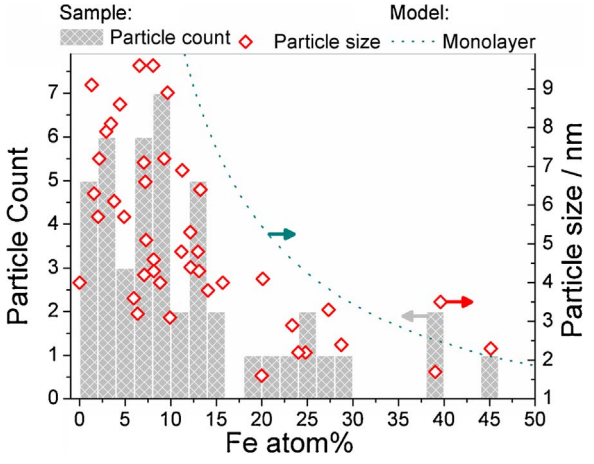

Fig. 4. Fe atom% distribution histogram obtain the EDS-STEM analysis and its correlation with particles size for $Pt_1Fe_{0.2}/SiO_2$_4C catalyst; the dashed line indicates the dependency of Fe/Pt ratio as a function of particle diameter (Pt core + Fe shell) at 100% surface coverage calculated through a geometric half-spherical model.

of 3d metals solely by the edge position [36], the overall XANES features of the $Pt_1Fe_{0.2}/SiO_2$_4C indicates that Fe is present in high oxidation state before reduction. An alternative method to estimate the overall Fe oxidation state in this type of system, where typical bulk standards are not expected to match, has been proposed by Capehart [33] based on the integrated area of the spectrum near the energy threshold, in comparison with standards with known oxidation states, as shown in Fig. 6. This analysis gave an oxidation state of about 2.8+ state for the fresh $Pt_1Fe_{0.2}/SiO_2$_4C, Fig. 6. These results, together with the attenuated features above the edge, Fig. 5a, are in agreement with the presence of well dispersed FeO_x species.

The TPR-XANES results, Fig. 5c, show the reduction of the FeO_x species at about 408 K, without further evolution up to 873 K. As expected, the final spectrum does not show a good match with any of the bulk standards (Fig. 5b), with features resembling both FeO and Fe. Although the pre-edge region (~7112 eV) is shifted towards FeO, the white-line (~7128 eV) is significantly attenuated, as for metallic Fe. Studies of FePt alloys [37,38] showed in general that the Fe is electron deficient due to charge transfer to the Pt atoms; the XANES spectrum has a pre-edge feature similar to the Fe foil but a shoulder around 7126 eV and a shift of the oscillations after the edge associated with the presence of Pt neighbors. The calculated oxidation state suggests a 1.9+ average final state attributed to the presence of FeO_x species and/or Fe-Pt.

It is important to note that the Fe was re-oxidized to a state similar to the initial state when the catalyst was exposed at room temperature to 5% O_2, as seen in Fig. S5. This behavior shows that it is not possible to observe the actual species once the catalyst is passivated or briefly exposed to air. Furthermore, even with rigorous control of sample preparation for *ex situ* XANES measurements, under inert atmosphere and sealing, it was not possible to avoid oxidation of the iron (Fig. S6).

The Pt L_3-edge XANES before and after reduction can be seen in Fig. 7. Before reduction, the monometallic Pt/SiO_2 and $Pt_1Fe_{0.2}/SiO_2$_4C catalysts both show similar profiles to the Pt foil, but with slightly higher white line, see Fig. 7b, due to the nanometric size and passivation. After reduction, the profile is closer to the spectrum of the foil, with a slight tailing above the white line expected by the presence of adsorbed H_2 on the surface [39]. The first derivative of the spectra, Fig. 7c, shows that the energy edge position did not change, independent of the sample or the pretreatment, indicating that Pt is mostly reduced. No significant modification was detected after re-oxidation treatment performed at room temperature with 5% O_2/He, and the spectra resemble the initial state. These results confirm that the Pt L_3-edge spectrum was not sensitive to the presence of Fe. The qualitative information derived by XANES was confirmed by EXAFS analysis, Table S2. The first peak of the Fourier Transform (Fig. S7) of the fresh bimetallic catalyst has both Pt-O and Pt-Pt, while after reduction only the Pt–Pt phase is present. The EXAFS results were insensitive to the presence of Fe. All changes and observations for the $Pt_1Fe_{0.2}/SiO_2$_4C catalyst were similar to the ones observed on the monometallic Pt/SiO_2 catalyst, see Fig. S8.

In situ XANES measurements at Fe K-edge and Pt L_3-edge under WGSR, Fig. S9 and Fig. 7, showed that the phase under reaction conditions is similar to the phases after reduction. These results indicate that Fe species formed during reduction are likely present under WGSR conditions.

3.2. Reaction kinetics measurements

Catalytic activities for the WGSR are summarized on Table 1. The addition of Fe in consecutive cycles through the CSR method on the Pt/SiO_2 catalyst increases the rate of CO_2 production per active site (TOF). The promotion effect (rate of enhanced activity compared with Pt/SiO_2 catalysts) increases with the Fe up to 4.6 times on $Pt_1Fe_{0.2}/SiO_2$_4C. The $Pt_1Fe_{0.16}/SiO_2$_1C catalyst showed similar performance to the $Pt_1Fe_{0.2}/SiO_2$_4C catalyst. A Fe/SiO_2 catalyst (made by CSR in a one-step

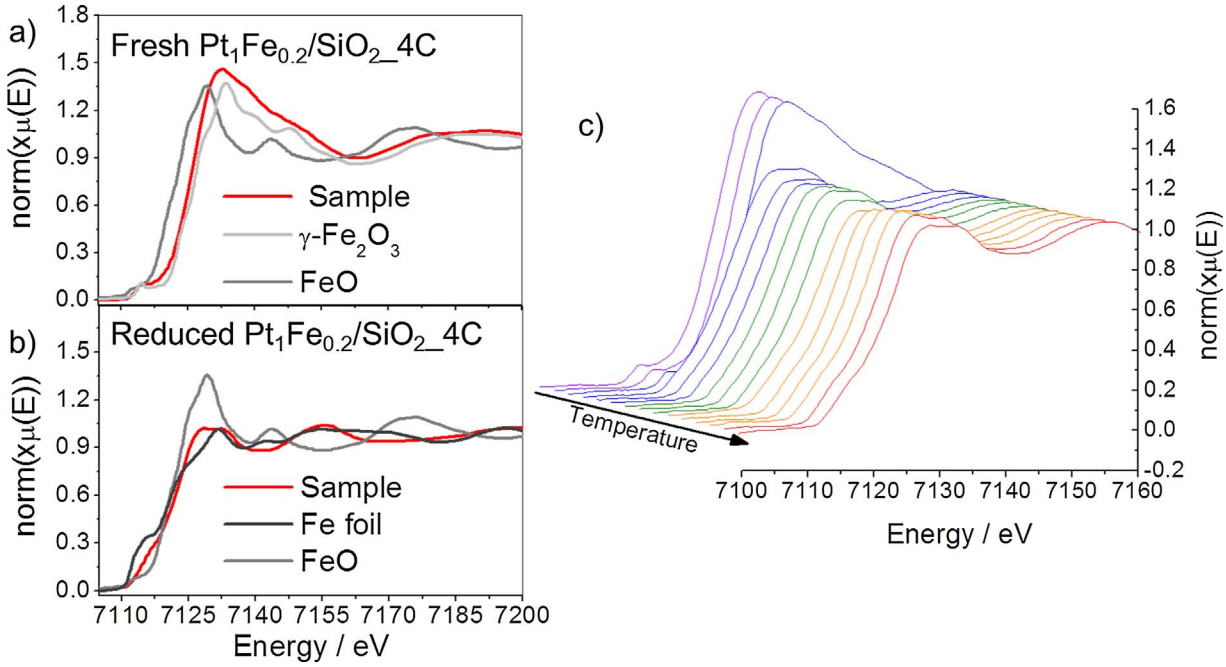

Fig. 5. a) XANES of the fresh $Pt_1Fe_{0.2}/SiO_2$_4C and b) reduced catalyst, in comparison to iron standards; c) TPR-XANES at the Fe K-edge for $Pt_1Fe_{0.2}/SiO_2$_4C.

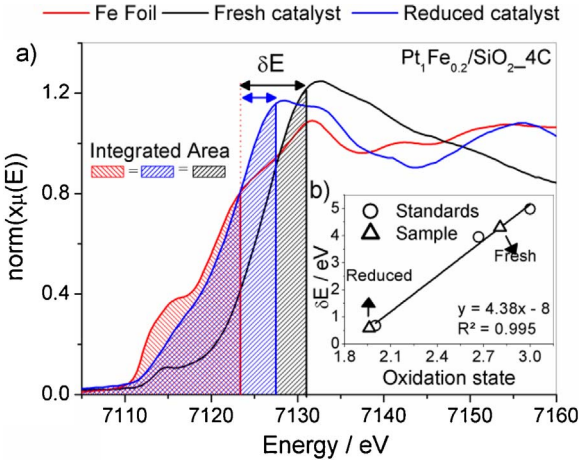

Fig. 6. a) XANES spectra of $Pt_1Fe_{0.2}/SiO_2$_4C catalyst (before and after reduction) and integrated areas compared to metallic Fe standard; b) correlation between δE and oxidation state obtained by the Capehart method [33].

deposition with Fe wt% similar to $Pt_1Fe_{0.2}/SiO_2$_4C) did not have any activity under the studied conditions. A physical mixture of the monometallic counterparts, Pt/SiO_2 and Fe/SiO_2, had similar activity to the Pt/SiO_2. These observations show that the promotion of Pt by Fe is caused by an intimate contact between FeO_x species and Pt.

To further quantify the promotion effect of the FeO_x phase, a Pt/C catalyst was made. This catalyst did not have any measureable activity at 543 K under the same conditions as Pt/SiO_2, even when 20 times more catalyst was used (2.1 g of Pt/C). The promotion of Fe increased the reactivity but its activity was lower than the silica supported catalysts. It was necessary to increase the reaction temperature to 623 K and increase the water content from 1 CO : $2H_2O$ to 1 CO : $3H_2O$ to detect activity and avoid the formation of Fe-carbides, which catalyze CO hydrogenation reactions [40]. At these conditions, the $Fe_1Pt_{0.2}$/C_1C was 33 times more active than its monometallic counterpart. These results confirm that the hydroxyls group on the SiO_2 support play a key role in the WGSR, impacting also in the promotion effect by the FeO_x species.

4. Discussion

4.1. Synthesis

The basis of the controlled surface reaction (CSR) technique is to add a metallic precursor selectively on the surface of a previously deposited metallic NP through reaction. In previous work [12–16], it was proposed that hydrogen pretreatment was necessary to clean the catalyst surface − degasing of oxygen and water − and also to cover the surface of the first metal with hydrogen, which could then react with a low-valence organometallic complex. The CSR method requires the precursor to react at the NP surface or near it, so carbonyl complexes containing alkene ligands are usually selected.

For these complexes, the reaction at the surface could take place through the interaction of hydride-like species bonded to surface Pt atoms with the alkenes [41,42] or by the abstraction of CO molecules by the NP. Both pathways generate coordinatively unsaturated species that could undergo decomposition pathways, depositing onto the NP. The organometallic precursor could also react directly with the hydroxyls of the support, even if non-specific adsorption is observed when the pure support is subjected to the CSR process; in this case, OH groups near the Pt-NPs could react with precursor species.

Here, the (cyclohexadiene)iron tricarbonyl was chosen as the iron source based on previous work [12–16], in which organotransition complexes containing carbonyl groups and alkene ligands presents the proper combination of stability, due to the backbonding of the ligands, so it would not react with the support, and sufficient reactivity such that it interacts with the NPs. Initial studies using (cyclooctatetraene) iron tricarbonyl and cyclopentadienyliron dicarbonyl dimer did not lead to selective deposition of Fe on the Pt surface. These results indicate that a complex such as (cyclohexadiene)iron tricarbonyl, with the half-sandwich/piano stool geometry with an alkene with low degree of unsaturation, presents an effective compromise between reactivity and selectivity. Indeed, we could successfully produce FePt catalysts on SiO_2 and C supports by CSR using this complex. Nevertheless, its use in other supports, such as Al_2O_3 and TiO_2, did not succeed, suggesting that the acidity/strength of OH surface groups of the support may impose other requirements to the complex to inhibit its undesired decomposition on the support. This limitation is an important issue that has still to

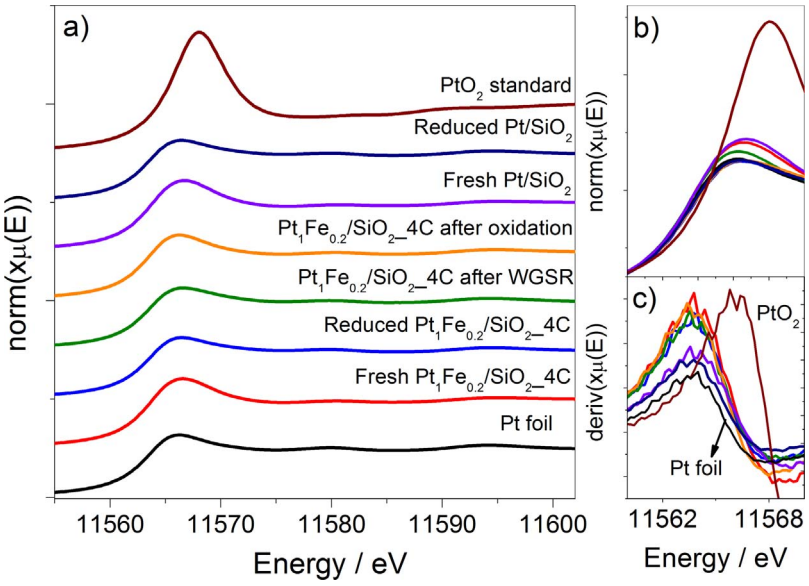

Fig. 7. a) XANES spectra on the Pt L_3-edge of the $Pt_1Fe_{0.2}/SiO_2$_4C catalyst; b) zoomed in view of the absorption edge; and c) first derivative of the XANES spectra.

Table 1
Characterization and catalytic activity of catalysts in WGSR, 10% CO and 20% H2O at 543 K.

Catalyst	CO uptake / μmol g^{-1}	CO_2 production rate[a] / μmol g_{Pt}^{-1} min^{-1}	TOF[b] / 10^{-3} s^{-1}
Fe/SiO_2	-	0	0
Pt/SiO_2	49	659	10.4
Physical mixture[c]	-	511	7.2
$Pt_1Fe_{0.06}/SiO_2$_1C	32	590	15.3
$Pt_1Fe_{0.1}/SiO_2$_2C	30	839	25.8
$Pt_1Fe_{0.2}/SiO_2$_4C	27	1525	47.5
$Pt_1Fe_{0.16}/SiO_2$_1C	29	1503	48.9
Pt/C	95	0 (170[d])	0 (1.5[d])
$Pt_1Fe_{0.2}$/C_1C	76	89 (4455[d])	1.5 (48.5[d])

[a] CO_2 production rate in μmol of CO_2 per g of Pt per minute.
[b] Estimated from CO uptake, assuming 1:1 CO:Pt stoichiometry.
[c] Physical mixture of monometallic Pt and Fe catalysts, with the amounts of Pt and Fe equivalent to $Pt_1Fe_{0.2}/SiO_2$_4C.
[d] Reaction performed with 8% CO, 24% H_2O, and He as balance to 100 mL min^{-1} at 623 K.

be better evaluated to allow the translation of the method to a broad set of supports.

For the bare SiO_2 support, no Fe deposition could be detected by UV–vis, suggesting that in this case the OH groups on the support were inactive. However, the scenario was different in the presence of Pt NPs, and the results suggest that the OH surface groups near the Pt sites play an important role in the FePt system. The similar adsorption achieved in the first cycle by the Pt/SiO_2 catalyst treated under vacuum or under H_2 indicates that activation of the surface by H was not necessary in this first cycle. Since the OH groups on the support were inactive, this behavior suggests that the Fe precursor is mostly deposited onto hydroxyl groups at the Pt-SiO_2 interface or at the Pt surface. When a simple half spherical geometrical model was applied, the percentage of the Pt atoms on the perimeter over the total amount of surface atoms was around 20–30% for NPs in the range of 4–6 nm, and this value is of the order of the amount of Fe deposited on the first cycle (around 15 μmol g^{-1}). In contrast, the hydrogen pretreatment had a crucial impact for the subsequent cycles. A rapid saturation was achieved in the second cycle when the Pt/SiO_2 catalyst was pretreated under vacuum, corresponding to a final coverage of about of half of the available Pt sites. In general, however, the regeneration of the adsorption sites observed with the reductive pretreatment between cycles may occur in different ways. Since the reactivity depends on the local Pt coordination (interface, kinks, edges, etc) a reconstruction of the Pt surface at each cycle cannot be ruled out. Nevertheless, the fact that it was possible to exceed the equivalent of one monolayer coverage after the 4th CSR cycle, while CO chemisorption showed that half of the Pt sites were site available, indicates a more complex mechanism. Another important piece of information to be considered is the similar results obtained by the CO chemisorption of multiple and single cycle CSR catalysts ($Pt_1Fe_{0.2}/SiO_2$_4C and $Pt_1Fe_{0.16}/SiO_2$_1C) as well as for the IWI catalyst (Table S3).

Platinum is known to form bimetallic alloys with a large set of metal, including Fe [43]. It has been shown in the literature that surface migration can happen in bimetallic system, where the topmost layer is terminated by the element with lower surface energy [44]. However, this equilibrium can be shifted in supported nanoparticles, due to the interaction with the support and the higher contribution that the surface energy term has in NPs. In addition, when exposing the bimetallic catalyst to different atmospheres, the equilibrium is affected. In the case of the CoPt system, for example, exposure to different atmospheres and nanometer particle size effects lead to surface reconstruction, where under O_2 the formation of CoO_x species is favored and under H_2 a Pt-rich surface is found [45]. Surface studies on the $Pt_{0.8}Fe_{0.2}$ (111) showed that Pt-Fe alloys exhibit a stronger tendency to form an ordered phase when compared to Pt-Co and Pt-Ni. Importantly, non-equivalent Pt sites are exposed at the surface due to the partially ordered alloy submonolayer [46].

A plausible mechanism for the effect of H_2 pretreatment on the effectiveness of Fe deposition is that part of the Fe species migrate to the Pt sub-surface, regenerating the reactive Pt sites [47]. Based on the *in situ* TPR-XANES results, however, part of the Fe species remains as FeO_x species. These species are likely to be localized near the Pt/SiO_2 interface and with the H_2 pretreatment the hydroxyl groups could be regenerated [48]. Both scenarios would be in agreement with the small decrease of the CO chemisorption after the first CSR cycle. Surface studies show that the FeO-Pt(111) system is characterized by a strong interaction [48]. In addition, once the catalyst is passivated, most of the Fe species become fully oxidized, as shown by XANES. Therefore, it cannot be rule out that under reduction pretreatment, before CO chemisorption or catalytic reaction, a rearrangement of the surface atomic species might occur due to the competition of different interactions: Fe-O-Si, Fe-O-Fe, Fe-O-Pt, Fe-Pt. This strong interaction could explain the similar results obtained with $Pt_1Fe_{0.16}/SiO_2$_1C and IWI-$Pt_1Fe_{0.2}/SiO_2$ catalysts, by driving a preferential deposition nearby the Pt NPs and rearrangement during the H_2 pretreatment. Liu et al. [49] studied FePt/Al_2O_3 catalyst and found that FeO_x species strongly interact with Pt,

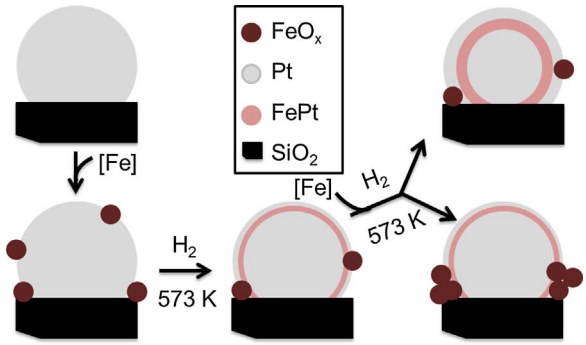

Scheme 1. CSR representation of the Fe precursor deposition onto Pt.

being found mostly in the vicinity of the Pt NPs. Tomita et al. [50] showed that the presence of water vapor, which could be generated *in situ* during reduction, helps to bring the FeO_x moieties and Pt in close contact in $FePt/Al_2O_3$ catalysts.

Putting this information together, the results suggest that FeO_x species were successfully deposited on Pt NPs by CSR. The Fe loading could be selectively increased by multiple-cycles, and at each cycle the Fe precursor deposits onto the renewed active Pt sites. The H_2 pretreatment is responsible for surface restructuring of the NPs with formation of FeO_x surface species and partial migration of the Fe to the subsurface; these effects would contribute to regenerate the Pt active sites. Subsequent CSR cycles increase the amount of segregated FeO_x and/or enrich the FePt phase. This behavior is summarized in Scheme 1.

4.2. Reaction kinetics measurements

It is known that the WSGR reaction can follow different pathways, grouped into two general mechanisms: associative or redox. In the first mechanism, a Langmuir-Hinshelwood type process is in place, where the adsorbed CO reacts with surface OH, generated by H_2O activation, going through carbonate/carboxylate or formate intermediates, e.g., Grabow et al. [51]. In the second mechanism, a Mars-Van Krevelen mechanism is observed, in which a redox support is involved and the CO oxidation takes place with a O from the support lattice, which is regenerated by the H_2O [52,53]. Recently, an associative mechanism with redox regeneration of OH groups has also been suggested to be favored in $Pt\text{-}CeO_2$ catalysts depending on the temperature [54,55]. In the case of monometallic catalysts, Pt/SiO_2 and Pt/C, the reaction takes place through the associative mechanism. It can be expected that the Pt/C catalyst behaves similar to metallic Pt, where H_2O activation is the rate-controlling step [51,52,56,57]; on the other hand, the better performance of Pt/SiO_2 catalyst under the same reaction conditions shows the important participation of the OH groups at the $Pt\text{-}SiO_2$ interface.

The deposition of Fe species on the Pt-based catalysts by CSR enhanced the WGSR activity. The lower activity of the physical mixture of catalysts (Pt/SiO_2 + Fe/SiO_2), the low temperature of Fe partial reduction found by *in situ* TPR-XANES experiments, and the reversible conversion between different iron oxidation states under mild condition are strong evidences of the creation of a FeO_x-Pt interface.

In the literature, the Fe promoting role [17,18,58–63] is often explained in terms of the redox properties of Fe, where Fe^{2+} can be oxidized to Fe^{3+} and be directly involved in the activation of water or oxygen. For example, CO oxidation studies on Pt and Au catalysts supported on different iron oxide phases showed that the $\gamma\text{-}Fe_2O_3$ phase led to better catalytic performance, which was associated with more facile conversion to the Fe_3O_4 phase and its redox properties [60]; a similar conclusion was obtained for the system Au/Fe_2O_3 applied in WGSR [23]. The role of the $Fe^{3+} \leftrightarrow Fe^{2+}$ pairs is similar to what is found in the Fe-based industrial high temperature shift (HTS) catalyst [64], where the Fe_3O_4 phase is the stable one under reaction conditions.

Surface studies on the FeO_x-Pt system have provided insights about the nature of the catalytic sites for CO oxidation. The FeO_x-Pt system is characterized by a strong metal support interaction and the formation of a FeO_x layer on Pt surface that enhances the CO oxidation by O_2 through a redox mechanism [65,66]. Knudsen et al. studied the reduction of FeO/Pt(111) surfaces and found that water is more easily activated in the FeO_x reduced structure in contrast to pristine FeO film, that was inert [48]. Fu et al. [63] showed that coordinatively unsaturated ferrous (CUF) sites confined at Pt interface are active at room temperature for CO oxidation. Direct evidence of these sites was provided by *in situ* scanning tunneling microscopy (STM) images [67]. These coordinatively unsaturated cations, found at the boundary of FeO_x nano-island deposits on the Pt surface, lead to a bifunctional mechanism, decreasing the energy barriers for O_2 activation and reaction with CO adsorbed on a nearby Pt site. It has been proposed that these sites are also highly active for H_2O activation, forming Fe_{CUF}-OH species and Fe-$O_{lattice}$H, which can then react with CO through an associative mechanism [68–70]. Lambrou et al. [71] also showed that the presence of Fe moieties in intimate contact with noble metals improves the CO surface coverage, favoring its adsorption due to electronic changes, playing a role as a donor of oxygen, and promoting oxidation reactions by surface diffusion of O*.

Regardless of the dominant mechanism, *in situ* XANES analysis during WGSR suggest that the FeO_x species remain highly dispersed and Fe is electron deficient (oxidation state $< 2+$). These results suggest that FeO_x species are capable of activating H_2O and promoting the reaction with CO adsorbed on a nearby Pt site. The weak impact of multiple CSR cycles on CO chemisorption but the almost linear increase of the TOF with Fe loading suggest that the FeO_x species are located mostly near the $Pt\text{-}SiO_2$ interface. Increasing the Fe loading likely modifies the vicinity of the Pt-NPs by forming small FeO_x clusters.

5. Conclusions

FePt catalysts were synthesized by controlled surface reactions, which allows for intimate contact between both metals, and were explored for the WGSR. We have studied the deposition mechanism by quantifying the effects of the acidity of the support, surface hydroxyl groups, and treatment atmosphere on the deposition of the Fe precursor compound, (cyclohexadiene)iron tricarbonyl. The nature of the deposition sites is suggested to be uncoordinated platinum atoms at edges and corners of the NPs and/or activated hydroxyl groups close to the NPs that can be renewed by hydrogen treatment.

Under catalytic conditions for WGSR, the Fe promotion was highlighted. When Fe was added to the Pt based catalysts, the WGSR TOF increased 5 times for the silica supported catalysts and 33 times for the carbon supported one. This showed that although the Fe promotion has a more significant impact on inert supports for WGSR, such as carbon, it also takes place in active WGSR supports, such as SiO_2, where the hydroxyl groups participate in the WGSR mechanism. This was confirmed by studies performed with this system on reactions, such as hydrogenation [34] and CO oxidation [35] where the Fe promotion was several orders of magnitude higher.

Acknowledgments

Work at UW was supported by the U.S. Department of Energy, Office of Basic Energy Sciences (DE-SC0014058). IBA and DZ acknowledge the São Paulo Research Foundation (FAPESP 2014/21988-7, 2015/20477-1 and 2015/23900-2) and National Council of Technological and Scientific Development (CNPq 140449/2014-0, 309373/2014-0 and 406879/2013-3) for financial support. We gratefully acknowledge M. Kumbhalkar, D.S. Gonçalves, T.M. Kokumai and T.E.R. Fiuza for their help with the synchrotron light measurements. We acknowledge the Brazilian Synchrotron Light Laboratory (LNLS), proposal 20160150, for the synchrotron light beamtime at the XAFS2 line.

This research used resources of the Advanced Photon Source, a U.S. Department of Energy (DOE) Office of Science User Facility operated for the DOE Office of Science by Argonne National Laboratory under Contract No. DE-AC02-06CH11357. The authors acknowledge use of instrumentation supported by UW MRSEC (DMR-1121288) and the UW NSEC (DMR-0832760).

Appendix A. Supplementary data

Supplementary data associated with this article can be found, in the online version, at http://dx.doi.org/10.1016/j.apcatb.2017.10.004.

References

[1] D.M. Alonso, S.G. Wettstein, J.A. Dumesic, Bimetallic catalysts for upgrading of biomass to fuels and chemicals, Chem. Soc. Rev. 41 (2012), http://dx.doi.org/10.1039/c2cs35188a.

[2] D. Gerceker, A.H. Motagamwala, K.R. Rivera-Dones, J.B. Miller, G.W. Huber, M. Mavrikakis, et al., Methane conversion to ethylene and aromatics on PtSn catalysts, ACS Catal. 7 (2017) 2088–2100, http://dx.doi.org/10.1021/acscatal.6b02724.

[3] J. Lee, Y.T. Kim, G.W. Huber, Aqueous-phase hydrogenation and hydrodeoxygenation of biomass-derived oxygenates with bimetallic catalysts, Green Chem. 16 (2014) 708, http://dx.doi.org/10.1039/c3gc41071d.

[4] A. Venugopal, J. Aluha, M.S. Scurrell, The water-Gas shift reaction over au-based, bimetallic catalysts. the Au-M (M = Ag, Bi, Co, Cu, Mn, Ni, Pb, Ru, Sn, Tl) on Iron (III) oxide system, Catal. Letters 90 (2003) 1–6, http://dx.doi.org/10.1023/A:1025872411739.

[5] K.D. Gilroy, A. Ruditskiy, H.-C. Peng, D. Qin, Y. Xia, Bimetallic nanocrystals: syntheses, properties, and applications, Chem. Rev. 116 (2016) 10414–10472, http://dx.doi.org/10.1021/acs.chemrev.6b00211.

[6] A. Choplin, L. Huang, A. Theolier, P. Gallezot, U. Siriwardane, S.G. Shore, et al., Formation of Fe-Os Fe-Ru, and Fe-Co bimetallic particles by thermal decomposition of heteropolynuclear clusters supported on a partially dehydroxylated magnesia, J. Am. Chem. Soc. 108 (1986) 4224–4225.

[7] A.S. Fung, M.R. McDevitt, P.A. Tooley, M.J. Kelley, D.C. Koningsberger, B.C. Gates, A model γ-Al_2O_3-supported Re-Pt catalyst prepared from [$Re_2Pt(CO)_{12}$] I. synthesis and spectroscopic characterization, J. Catal. 140 (1993) 190–208, http://dx.doi.org/10.1006/jcat.1993.1078.

[8] A.S. Fung, P.A. Tooley, M.R. McDevitt, B.C. Gates, M.J. Kelley, Supported metal catalysts prepared from bimetallic clusters: $ReOs_3$ clusters on γ-Al_2O_3, Polyhedron 7 (1988) 2421–2427, http://dx.doi.org/10.1016/S0277-5387(00)86362-7.

[9] B.C. Gates, Supported metal cluster catalysts, J. Mol. Catal. A Chem. 163 (2000) 55–65, http://dx.doi.org/10.1016/S1381-1169(00)00399-X.

[10] M.W. Small, S.I. Sanchez, L.D. Menard, J.H. Kang, A.I. Frenkel, R.G. Nuzzo, The atomic structural dynamics of gamma-Al_2O_3 supported Ir-Pt nanocluster catalysts prepared from a bimetallic molecular precursor: a study using aberration-corrected electron microscopy and X-ray absorption spectroscopy, J. Am. Chem. Soc. 133 (2011) 3582–3591, http://dx.doi.org/10.1021/ja110033g.

[11] A. Kulkarni, R.J. Lobo-Lapidus, B.C. Gates, Metal clusters on supports: synthesis, structure, reactivity, and catalytic properties, Chem. Commun. (Camb) 46 (2010) 5997–6015, http://dx.doi.org/10.1039/c002707n.

[12] C. Sener, T.S. Wesley, A.C. Alba-Rubio, M.D. Kumbhalkar, S.H. Hakim, F.H. Ribeiro, et al., PtMo bimetallic catalysts synthesized by controlled surface reactions for water gas shift, ACS Catal. 6 (2016) 1334–1344, http://dx.doi.org/10.1021/acscatal.5b02028.

[13] S.H. Hakim, C. Sener, A.C. Alba-Rubio, T.M. Gostanian, B.J. O'Neill, F.H. Ribeiro, et al., Synthesis of supported bimetallic nanoparticles with controlled size and composition distributions for active site elucidation, J. Catal. 328 (2015) 75–90, http://dx.doi.org/10.1016/j.jcat.2014.12.015.

[14] A.C. Alba-Rubio, C. Sener, S.H. Hakim, T.M. Gostanian, J.A. Dumesic, Synthesis of supported RhMo and PtMo bimetallic catalysts by controlled surface reactions, ChemCatChem 7 (2015) 3881–3886, http://dx.doi.org/10.1002/cctc.201500767.

[15] R. Carrasquillo-Flores, I. Ro, M.D. Kumbhalkar, S. Burt, C.A. Carrero, A.C. Alba-Rubio, et al., Reverse water-gas shift on interfacial sites formed by deposition of oxidized molybdenum moieties onto gold nanoparticles, J. Am. Chem. Soc. 137 (2015) 10317–10325, http://dx.doi.org/10.1021/jacs.5b05945.

[16] I. Ro, C. Sener, T.M. Stadelman, M.R. Ball, J.M. Venegas, S.P. Burt, et al., Measurement of intrinsic catalytic activity of Pt monometallic and Pt-MoOx interfacial sites over visible light enhanced $PtMoO_x/SiO_2$ catalyst in reverse water gas shift reaction, J. Catal. 344 (2016) 784–794, http://dx.doi.org/10.1016/j.jcat.2016.08.011.

[17] H. Zhang, D. Lin, G. Xu, J. Zheng, N. Zhang, Y. Li, et al., Facile synthesis of carbon supported Pt-nanoparticles with Fe-rich surface: a highly active catalyst for preferential CO oxidation, Int. J. Hydrogen Energy 40 (2015) 1742–1751, http://dx.doi.org/10.1016/j.ijhydene.2014.12.006.

[18] B. Qiao, A. Wang, L. Li, Q. Lin, H. Wei, J. Liu, et al., Ferric oxide-supported Pt subnano clusters for preferential oxidation of CO in H_2-rich gas at room temperature, ACS Catal. 4 (2014) 2113–2117, http://dx.doi.org/10.1021/cs500501u.

[19] H. Zhang, X. Liu, N. Zhang, J. Zheng, Y. Zheng, Y. Li, et al., Construction of ultrafine and stable PtFe nano-alloy with ultra-low Pt loading for complete removal of CO in PROX at room temperature, Appl. Catal. B Environ. 180 (2016) 237–245, http://dx.doi.org/10.1016/j.apcatb.2015.06.032.

[20] M. Kotobuki, T. Shido, M. Tada, H. Uchida, H. Yamashita, Y. Iwasawa, et al., XAFS characterization of Pt-Fe/zeolite catalysts for preferential oxidation of CO in hydrogen fuel gases, Catal. Letters 103 (2005) 263–269, http://dx.doi.org/10.1007/s10562-005-7163-5.

[21] R.F. XinshengLiu, O. Korotkikh, Selective catalytic oxidation of CO in H_2: structural study of Fe oxide-promoted Pt/alumina catalyst, Appl. Catal. A Gen. 226 (2002) 293–303, http://dx.doi.org/10.1016/S0926-860X(01)00915-2.

[22] K. Liu, A. Wang, T. Zhang, Recent advances in preferential oxidation of CO reaction over platinum group metal catalysts, ACS Catal. 2 (2012) 1165–1178, http://dx.doi.org/10.1021/cs200418w.

[23] D. Andreeva, V. Idakiev, T. Tabakova, A. Andreev, R. Giovanoli, Low-temperature water-gas shift reaction on Auα-Fe_2O_3 catalyst, Appl. Catal. A Gen. 134 (1996) 275–283, http://dx.doi.org/10.1016/0926-860X(95)00208-1.

[24] S.T. Daniells, M. Makkee, J.A. Moulijn, The effect of high-temperature pre-treatment and water on the low temperature CO oxidation with Au/Fe_2O_3 catalysts, Catal. Letters 100 (2005) 39–47, http://dx.doi.org/10.1007/s10562-004-3083-z.

[25] S. Luo, L. Barrio, T.-D. Nguyen-Phan, D. Vovchok, A.C. Johnston-Peck, W. Xu, et al., Importance of low dimensional CeO_x nanostructures in Pt/CeO_x-TiO_2 catalysts for the water–gas shift reaction, J. Phys. Chem. C 121 (2017) 6635–6642, http://dx.doi.org/10.1021/acs.jpcc.6b12285.

[26] T.M. Kokumai, D.A. Cantane, G.T. Melo, L.B. Paulucci, D. Zanchet, VO_x-Pt/Al_2O_3 catalysts for hydrogen production, Catal. Today (2016), http://dx.doi.org/10.1016/j.cattod.2016.09.021.

[27] M. Faust, M. Dinkel, M. Bruns, S. Bräse, M. Seipenbusch, Support effect on the water gas shift activity of chemical vapor deposition-tailored-Pt/TiO_2 catalysts, Ind. Eng. Chem. Res. 56 (2017) 3194–3203, http://dx.doi.org/10.1021/acs.iecr.6b04512.

[28] B.M. Eropak, A.E. Aksoylu, A reliable power-law type kinetic expression for PROX over Pt-Sn/AC under fully realistic conditions, Catal. Commun. 95 (2017) 67–71, http://dx.doi.org/10.1016/j.catcom.2017.03.003.

[29] A.S. Duke, K. Xie, A.J. Brandt, T.D. Maddumapatabandi, S.C. Ammal, A. Heyden, et al., Understanding active sites in the water-gas shift reaction for Pt-Re catalysts on titania, ACS Catal. 7 (2017) 2597–2606, http://dx.doi.org/10.1021/acscatal.7b00086.

[30] T. Magadzu, M.C. Kung, H.H. Kung, M.S. Scurrell, J.H. Yang, J.D. Henao, Low temperature water-gas shift reaction over Au supported on anatase in the presence of copper: EXAFS/XANES analysis of gold-copper ion mixtures on TiO_2, J. Phys. Chem. C (2017), http://dx.doi.org/10.1021/acs.jpcc.6b11419 (acs.jpcc.6b11419).

[31] J.-H. Lin, P. Biswas, V.V. Guliants, S. Misture, Hydrogen production by water-gas shift reaction over bimetallic Cu-Ni catalysts supported on La-doped mesoporous ceria, Appl. Catal. A Gen. 387 (2010) 87–94, http://dx.doi.org/10.1016/j.apcata.2010.08.003.

[32] B. Ravel, M. Newville, ATHENA, ARTEMIS, HEPHAESTUS: data analysis for X-ray absorption spectroscopy using IFEFFIT, J. Synchrotron Radiat. 12 (2005) 537–541, http://dx.doi.org/10.1107/S0909049505012719.

[33] T.W. Capehart, J.F. Herbst, R.K. Mishra, F.E. Pinkerton, X-ray-absorption edge shifts in rare-earth–transition-metal compounds, Phys. Rev. B 52 (1995) 7907–7914, http://dx.doi.org/10.1103/PhysRevB.52.7907.

[34] I. Ro, I.B., Aragao, Z. Brentzel, Y., Liu, M. Ball, K. Rivera-Dones, et al. Intrinsic activity of interfacial sites for Pt-Fe and Pt-Mo catalysts in the hydrogenation of carbonyl groups, Under Revision (n.d.).

[35] I. Ro, I.B., Aragao, J.P. Chada, Y., Liu, K.R. Rivera-Dones, M.R. Ball et al., The Role of Pt-FexOy Interfacial sites for CO Oxidation, Under Revision (n.d.).

[36] C. Piquer, M.A. Laguna-Marco, A.G. Roca, R. Boada, C. Guglieri, J. Chaboy, Fe K-edge X-ray absorption spectroscopy study of nanosized nominal magnetite, J. Phys. Chem. C. 118 (2014) 1332–1346, http://dx.doi.org/10.1021/jp4104992.

[37] F.-J. Lai, H.-L. Chou, L.S. Sarma, D.-Y. Wang, Y.-C. Lin, J.-F. Lee, et al., Tunable properties of Pt_xFe_{1-x} electrocatalysts and their catalytic activity towards the oxygen reduction reaction, Nanoscale 2 (2010) 573, http://dx.doi.org/10.1039/b9nr00239a.

[38] S.J.A. Figueroa, S.J. Stewart, T. Rueda, A. Hernando, P. de la Presa, Thermal evolution of Pt-rich FePt/Fe_3O_4 heterodimers studied using X-ray absorption near-edge spectroscopy, J. Phys. Chem. C. 115 (2011) 5500–5508, http://dx.doi.org/10.1021/jp111591p.

[39] N. Guo, B.R. Fingland, W.D. Williams, V.F. Kispersky, J. Jelic, W.N. Delgass, et al., Determination of CO, H_2O and H_2 coverage by XANES and EXAFS on Pt and Au during water gas shift reaction, Phys. Chem. Chem. Phys. 12 (2010) 5678, http://dx.doi.org/10.1039/c000240m.

[40] G.P. van der Laan, A.A.C.M. Beenackers, Intrinsic kinetics of the gas-solid Fischer-Tropsch and water gas shift reactions over a precipitated iron catalyst, Appl. Catal. A Gen. 193 (2000) 39–53, http://dx.doi.org/10.1016/s0926-860x(99)00412-3.

[41] X. Li, G. Li, W. Zang, L. Wang, X. Zhang, Catalytic activity of shaped platinum nanoparticles for hydrogenation: a kinetic study, Catal. Sci. Technol. 4 (2014) 3290, http://dx.doi.org/10.1039/C4CY00580E.

[42] S. Ikeda, S. Ishino, T. Harada, N. Okamoto, T. Sakata, H. Mori, et al., Ligand-free platinum nanoparticles encapsulated in a hollow porous carbon shell as a highly active heterogeneous hydrogenation catalyst, Angew. Chemie. 118 (2006) 7221–7224, http://dx.doi.org/10.1002/ange.200602700.

[43] A.V. Ruban, H.L. Skriver, J.K. Nørskov, Surface segregation energies in transition-metal alloys, Phys. Rev. B 59 (1999) 15990–16000, http://dx.doi.org/10.1103/PhysRevB.59.15990.

[44] Y. Xu, A.V. Ruban, M. Mavrikakis, Adsorption and dissociation of O_2 on Pt-Co and Pt-Fe alloys, J. Am. Chem. Soc. 126 (2004) 4717–4725, http://dx.doi.org/10.1021/ja031701+.

[45] V. Papaefthimiou, T. Dintzer, V. Dupuis, A. Tamion, F. Tournus, D. Teschner, et al.,

When a metastable oxide stabilizes at the nanoscale: wurtzite CoO formation upon dealloying of PtCo nanoparticles, J. Phys. Chem. Lett. 2 (2011) 900–904, http://dx.doi.org/10.1021/jz2003155.
[46] P. Beccat, Y. Gauthier, R. Baudoing-Savois, J.C. Bertolni, Monotonous concentration profile and reconstruction at $Pt_{80}Fe_{20}$(111): LEED study of a catalyst, Surf. Sci. 238 (1990) 105–118, http://dx.doi.org/10.1016/0039-6028(90)90069-K.
[47] U. Bardi, The atomic structure of alloy surfaces and surface alloys, Reports Prog. Phys. 57 (1994) 939–987, http://dx.doi.org/10.1088/0034-4885/57/10/001.
[48] J. Knudsen, L.R. Merte, L.C. Grabow, F.M. Eichhorn, S. Porsgaard, H. Zeuthen, et al., Reduction of FeO/Pt(111) thin films by exposure to atomic hydrogen, Surf. Sci. 604 (2010) 11–20, http://dx.doi.org/10.1016/j.susc.2009.10.008.
[49] X. Liu, O. Korotkikh, R. Farrauto, Selective catalytic oxidation of CO in H_2: Structural study of Fe oxide-promoted Pt/alumina catalyst, Appl. Catal. A Gen. 226 (2002) 293–303, http://dx.doi.org/10.1016/S0926-860X(01)00915-2.
[50] A. Tomita, K. Shimizu, K. Kato, Y. Tai, Pt/Fe-containing alumina catalysts prepared and treated with water under moderate conditions exhibit low-temperature CO oxidation activity, Catal. Commun. 17 (2012) 194–199, http://dx.doi.org/10.1016/j.catcom.2011.11.007.
[51] L.C. Grabow, A.A. Gokhale, S.T. Evans, J.A. Dumesic, M. Mavrikakis, Mechanism of the water gas shift reaction on Pt: first principles, experiments, and microkinetic modeling, J. Phys. Chem. C 112 (2008) 4608–4617, http://dx.doi.org/10.1021/jp7099702.
[52] C.M. Kalamaras, G.G. Olympiou, A.M. Efstathiou, The water-gas shift reaction on Pt/γ-Al_2O_3 catalyst: operando SSITKA-DRIFTS-mass spectroscopy studies, Catal. Today 138 (2008) 228–234, http://dx.doi.org/10.1016/j.cattod.2008.06.010.
[53] G.K. Reddy, P.G. Smirniotis, Water Gas Shift Reaction Research Developments and Applications, 1st ed., Elsevier B.V., 2015.
[54] C.M. Kalamaras, I.D. Gonzalez, R.M. Navarro, J.L.G. Fierro, A.M. Efstathiou, Effects of reaction temperature and support composition on the mechanism of water-gas shift reaction over supported-Pt catalysts, J. Phys. Chem. C 115 (2011) 11595–11610, http://dx.doi.org/10.1021/jp201773a.
[55] S. Aranifard, S.C. Ammal, A. Heyden, On the importance of metal–oxide interface sites for the water–gas shift reaction over Pt/CeO_2 catalysts, J. Catal. 309 (2014) 314–324, http://dx.doi.org/10.1016/j.jcat.2013.10.012.
[56] M. Stamatakis, Y. Chen, D.G. Vlachos, First-principles-based kinetic monte carlo simulation of the structure sensitivity of the water-gas shift reaction on platinum surfaces, J. Phys. Chem. C 115 (2011) 24750–24762, http://dx.doi.org/10.1021/jp2071869.
[57] C.M. Kalamaras, S. Americanou, A.M. Efstathiou, Redox vs associative formate with OH group regeneration WGS reaction mechanism on Pt/CeO_2: Effect of platinum particle size, J. Catal. 279 (2011) 287–300, http://dx.doi.org/10.1016/j.jcat.2011.01.024.
[58] C. Wang, H. Daimon, S. Sun, Dumbbell-like Pt-Fe_3O_4 nanoparticles and their enhanced catalysis for oxygen reduction reaction, Nano Lett. 9 (2009) 1493–1496, http://dx.doi.org/10.1021/nl8034724.
[59] A. Luengnaruemitchai, K. Srihamat, C. Pojanacaraphan, R. Wanchanthuek, Activity of Au/Fe_2O_3-TiO_2 catalyst for preferential CO oxidation, Int. J. Hydrogen Energy 40 (2015) 13443–13455, http://dx.doi.org/10.1016/j.ijhydene.2012.12.009.
[60] K. Zhao, H. Tang, B. Qiao, L. Li, J. Wang, High activity of Au/γ-Fe_2O_3 for CO oxidation: effect of support crystal phase in catalyst design, ACS Catal. 5 (2015) 3528–3539, http://dx.doi.org/10.1021/cs5020496.
[61] X. Yang, A. Wang, B. Qiao, J. Li, J. Liu, T. Zhang, Single-atom catalysts: a new frontier in heterogeneous catalysis, Acc. Chem. Res. 46 (2013) 1740–1748, http://dx.doi.org/10.1021/ar300361m.
[62] G. Li, L. Li, B. Wu, J. Li, Y. Yuan, J. Shi, Controlled one-step synthesis of Pt decorated octahedral Fe_3O_4 and its excellent catalytic performance for CO oxidation, Nanoscale 7 (2015) 17855–17860, http://dx.doi.org/10.1039/C5NR05933J.
[63] Q. Fu, W. Li, Y. Yao, H. Liu, H. Su, D. Ma, et al., Interface-confined ferrous centers for catalytic oxidation, Science 328 (2010) 1141–1144, http://dx.doi.org/10.1126/science.1188267.
[64] M. Zhu, I.E. Wachs, Iron-based catalysts for the high-temperature water-gas shift (HT-WGS) reaction: a review, ACS Catal. 6 (2016) 722–732, http://dx.doi.org/10.1021/acscatal.5b02594.
[65] Y.-N. Sun, Z.-H. Qin, M. Lewandowski, E. Carrasco, M. Sterrer, S. Shaikhutdinov, et al., Monolayer iron oxide film on platinum promotes low temperature CO oxidation, J. Catal. 266 (2009) 359–368, http://dx.doi.org/10.1016/j.jcat.2009.07.002.
[66] M. Lewandowski, Y.N. Sun, Z.-H. Qin, S. Shaikhutdinov, H.-J. Freund, Promotional effect of metal encapsulation on reactivity of iron oxide supported Pt catalysts, Appl. Catal. A Gen. 391 (2011) 407–410, http://dx.doi.org/10.1016/j.apcata.2010.04.030.
[67] W. Kudernatsch, G. Peng, H. Zeuthen, Y. Bai, L.R. Merte, L. Lammich, et al., Direct visualization of catalytically active sites at the FeO–Pt(111) interface, ACS Nano 9 (2015) 7804–7814, http://dx.doi.org/10.1021/acsnano.5b02339.
[68] Y. Jin, G. Sun, F. Xiong, L. Ding, W. Huang, Water-activated lattice oxygen in FeO (111) islands for low-temperature oxidation of CO at Pt-FeO interface, J. Phys. Chem. C 120 (2016) 9845–9851, http://dx.doi.org/10.1021/acs.jpcc.6b02256.
[69] L. Xu, Y. Ma, Y. Zhang, Z. Jiang, W. Huang, Direct evidence for the interfacial oxidation of CO with hydroxyls catalyzed by Pt/Oxide nanocatalysts, J. Am. Chem. Soc. 131 (2009) 16366–16367, http://dx.doi.org/10.1021/ja908081s.
[70] W. Wang, H. Zhang, W. Wang, A. Zhao, B. Wang, J.G. Hou, Observation of water dissociation on nanometer-sized FeO islands grown on Pt(111), Chem. Phys. Lett. 500 (2010) 76–81, http://dx.doi.org/10.1016/j.cplett.2010.09.080.
[71] P.S. Lambrou, P.G. Savva, J.L.G. Fierro, A.M. Efstathiou, The effect of Fe on the catalytic behavior of model Pd-Rh/CeO_2-Al_2O_3 three-way catalyst, App. Catal. B Environ. 76 (2007) 375–385, http://dx.doi.org/10.1016/j.apcatb.2007.06.004.